NASA TECHNICAL NOTE

NASA TN D-8523

NASA TN D-8523

A SUSPENDED ANEMOMETER SYSTEM FOR MEASURING TRUE AIRSPEED ON LOW-SPEED AIRPLANES

David D. Kershner

Langley Research Center
Hampton, Va. 23665

NATIONAL AERONAUTICS AND SPACE ADMINISTRATION • WASHINGTON, D. C. • OCTOBER 1977

1. Report No.	2. Government Accession No.	3. Recipient's Catalog No.
NASA TN D-8523		

4. Title and Subtitle	5. Report Date
A SUSPENDED ANEMOMETER SYSTEM FOR MEASURING TRUE AIRSPEED ON LOW-SPEED AIRPLANES	October 1977
	6. Performing Organization Code
7. Author(s)	8. Performing Organization Report No.
David D. Kershner	L-11269
	10. Work Unit No.
9. Performing Organization Name and Address	505-07-41-06
NASA Langley Research Center Hampton, VA 23665	11. Contract or Grant No.
	13. Type of Report and Period Covered
12. Sponsoring Agency Name and Address	Technical Note
National Aeronautics and Space Administration Washington, DC 20546	14. Sponsoring Agency Code

15. Supplementary Notes

16. Abstract

A suspended anemometer system for calibrating pitot-static systems on low-speed research airplanes is described. The anemometer measures true airspeed when suspended beneath the airplane on a long cable in regions of undisturbed air. The electrical output of the propeller-driven tachometer is a sine wave, the frequency of which is proportional to true airspeed. The anemometer measures true airspeed over a range from 20 to 60 m/sec (40 to 120 knots) at altitudes to 3000 m, with an accuracy of ±0.5 percent of full-scale range. This accuracy is exclusive of errors in the recording system. The stability of the suspended system was investigated and was found adequate in the airspeed range. For the purpose of determining the location of the anemometer relative to the airplane, a method is given for calculating the shape assumed by the deployed cable.

17. Key Words (Suggested by Author(s))	18. Distribution Statement
Airspeed calibration Anemometer Flight instrumentation Instrumentation	Unclassified - Unlimited Subject Category 06

19. Security Classif. (of this report)	20. Security Classif. (of this page)	21. No. of Pages	22. Price*
Unclassified	Unclassified	28	$4.00

* For sale by the National Technical Information Service, Springfield, Virginia 22161

A SUSPENDED ANEMOMETER SYSTEM FOR MEASURING TRUE AIRSPEED ON LOW-SPEED AIRPLANES

David D. Kershner
Langley Research Center

SUMMARY

A suspended anemometer system for calibrating pitot-static systems on low-speed research airplanes is described. The anemometer measures true airspeed when suspended beneath the airplane on a long cable in regions of undisturbed air. The electrical output of the propeller-driven tachometer is a sine wave, the frequency of which is proportional to true airspeed. The anemometer measures true airspeed over a range from 20 to 60 m/sec (40 to 120 knots) at altitudes to 3000 m, with an accuracy of $\pm$0.5 percent of full-scale range. This accuracy is exclusive of errors in the recording system. The stability of the suspended system was investigated and was found adequate in the airspeed range. For the purpose of determining the location of the anemometer relative to the airplane, a method is given for calculating the shape assumed by the deployed cable.

INTRODUCTION

Impact pressure is sensed in modern airplanes by measuring the difference between total pressure and static pressure. The total-pressure probe can be located at any convenient place where the energy of the airstream is unaffected by external heating, by wakes from protuberances, or by the boundary layer. Static pressure is influenced by the airplane flow field and is sensed by flush-static ports on the fuselage skin or static tubes, the locations of which are determined by flight and wind-tunnel data. Such systems are calibrated on the full-scale airplane prototypes by several methods, including one in which the airplane static source is compared with one obtained from a cone-stabilized static-pressure source which is trailed in undisturbed air far behind the airplane. (See ref. 1.) Dynamic pressure can also be computed from free-stream measurements of true airspeed and free-air temperature. An anemometer was developed for use in research programs on general aviation airplanes. The operating range of these airplanes is approximately 20 to 60 m/sec (40 to 120 knots) at altitudes from sea level to 3000 m.

In the early years of airplane instrumentation, airspeed calibrations were made with streamlined devices suspended beneath the airplane, as summarized in references 2 and 3. Some devices simply sensed static pressure in the undisturbed air. The popularity of the concept was limited by a combination of three factors: (1) problems with deployment and stability of the suspended systems, (2) the difficulty of accurately recording the output under airplane environmental conditions, and (3) in the case of the propeller anemometer, the dependence of the calibration on air density brought on by loads in the generator.

The anemometer system described in this paper is similar in concept to the early anemometers, but the use of currently available components overcome some of the hazards and operating problems. For example, the availability of the small-size electromechanical pickup allows a reduction in the size of the anemometer and support cable. It is shown herein that the small-diameter cable does not trail back as much, thus providing greater separation between the anemometer and the airplane. Additionally, the thinner-cable system is more stable.

The use of the anemometer in flight testing of low-speed airplanes is discussed in reference 4, which includes the theory of calibrating airplane pitot-static systems, the derivation of pertinent equations, and a brief discussion of several other techniques. The present paper contains a description of the system, its operation, the design considerations, the accuracy and calibration techniques, the cable shape, and the stability boundaries.

SYMBOLS

a	slope of lift curve of anemometer tail, rad^{-1}
C_D	effective drag coefficient of cable and anemometer (ref. 5)
D	drag per unit vertical length of cable, N/m
D_a	drag of anemometer, N
e	partial pressure of water vapor, Pa
f	frequency of oscillation, Hz
k	radius of gyration of anemometer, m
l	tail length of anemometer, m
p	static pressure, Pa
q	dynamic pressure (total pressure less static pressure) assumed equivalent to impact pressure, $\rho V^2/2$, Pa
S	surface area of anemometer tail, m^2
s	length of cable, m
T	tension in cable, N
t	temperature, K
V	true airspeed, m/sec or knots
w	weight of anemometer, N
x	longitudinal coordinate, m

z vertical coordinate, m

ρ air density, kg/m^3

ϕ angle from cable element to horizontal, deg

Subscripts:

i initial

o sea-level conditions

DESCRIPTION OF SYSTEM

Anemometer

The construction of the anemometer is shown in figures 1, 2, and 3. The streamlined brass body provides for the stabilizing tail, the propeller-tachometer unit, and for the entry and attachment of the supporting cable. The weight of the anemometer is 0.77 kg and the length is 0.20 m. The shape of the streamlined body is that of a C-class airship hull. (See ref. 6.) The low fineness ratio of the body maximizes tension in the cable for a given moment of inertia of the body. The propeller-tachometer assembly was extended forward of the anemometer body to produce a bottle-nosed appearance. This shape is needed to achieve a linear airspeed calibration. The middle of the body is made in two pieces (fig. 2), the smaller, or cap piece, being hollowed out to make room for the cable attachment and electrical terminations. The cable is routed through the tapered hole in the main or upper half of the body. The cable is two-conductor coaxial with the central conductor being of stranded steel. A layer of insulation separates the central conductor from a woven copper sleeving, and an outside plastic insulation covering completes the cable assembly. Its overall diameter is 1.4 mm. At the end of the cable, the sleeving is separated from the stranded-steel central conductor, and electrical connection is made to the electromagnetic pickup. A metal ring is swaged to the tip of the central conductor to secure the anemometer to the cable. The anemometer body is bored to receive the propeller-tachometer assembly and slotted to receive the shroud supports.

Propeller-Tachometer Assembly

The propeller-tachometer assembly is shown in figure 4. The propeller measures 31.75 mm in diameter and is made of cast aluminum by the lost-wax investment-casting method. The hub has a streamlined, near hemi-ellipsoid shape. The hub is hollowed to reduce the mass for increased responsiveness to dynamic inputs. The propeller fits on the tachometer shaft and is secured with a set screw. The blades are flat, six in number, and are cast integrally with the hub, with a blade angle of 45° to the longitudinal axis. The tachometer shaft runs in a pair of low-friction ball-bearing assemblies and has a mild-steel six-tooth wheel attached. The rotation of the toothed wheel produces a nearly sinusoidal electrical output from the electromagnetic pickup, the frequency of which is proportional to true airspeed over the desired range of 20 to 60 m/sec (40 to

120 knots). The output measures approximately 3 V peak and 1200 Hz at maximum airspeed. All of the tachometer components are contained in the housing as shown in figure 4, and the whole assembly fits into the anemometer (fig. 3) and is held with a locked set screw. A stainless-steel shroud (figs. 2 and 3) protects the propeller from damage during handling, as well as during cradling in flight. The lip on the shroud is shaped to reduce the flow loss with misalinement. The shroud is mounted on four supports and is secured by high-temperature solder.

Tail Fin

The tail fin (fig. 3) is of welded-aluminum construction. The support shaft is slotted to receive the cross plates that are set normal to each other. The 100-mm-diameter sheet-metal ring is bent into shape, and the whole unit is welded together. The tail is mounted by inserting the end of the shaft into the body and securing it with a locked set screw. Static balance is achieved by adjusting insertion depth before tightening the set screw.

Deployment Mechanism and Control Unit

The deployment mechanism deploys and retracts the anemometer under the complete control of an operator in the airplane. Figure 5 is an exterior view of the complete system with the anemometer retracted. A streamlined cover protects the deployment mechanism from dirt and keeps the airflow uniform. Side views of the deployment mechanism with the cover removed (fig. 6) show some of the construction details. Attachment to the airplane is made by the flange, and the electrical connections are made to the terminal on the mechanism visible in figure 6(b). The operation of the mechanism is explained in conjunction with figure 7. It will be noted from figure 7(a) that the cable supply spool is of complex design because the cable is serving both electrical and mechanical functions. Electrical continuity from the rotating spool is made with slip rings, which are attached to one end of the spool shaft. The end of the cable is held fast to the spool with a clip and is soldered to the slip-ring wires which are drawn through the hollow shaft. These details are not shown in figure 7(a), but the solder terminals and clamp are in the insulating core on the end that is shown covered by wraps of cable. On the other end of the supply spool, some of the details of design are shown in cross-section view. The driven shaft of the spool is not attached directly to the spool but through a concentric, torsional spring, as shown. The spring absorbs the energy in the rotating spool when it stops at the completion of retraction. Electrical power is removed from the motor when the cradle switch (fig. 7(b)) is engaged by the retracted anemometer. At that instant, the cable length is fixed and would stop with a damaging jerk were it not for the torsional-spring coupling between the shaft and spool. After most of the cable has run off the spool and the final layer is reached, the end-of-roll switch is set to remove power from the motor to prevent overrun and reverse wrapping. The spool is driven by the motor through a worm gear and a set of beveled gears, shown in figure 6(a). The motor draws a steady direct current of 1.25 A operating from a 28 ± 3 V line with reverse-polarity capability. The motor is a permanent magnet-field type which produces a torque of about 3.5 N-cm when running at 6870 rpm. The anemometer is deployed at a rate of 1 m/sec and is retrieved at a rate of 0.6 m/sec. A level winder keeps the cable wrappings neat to get maximum capacity

on the spool. The leveler is driven through spur gears from the spool shaft shown in figures 6(b) and 7(a). The worm was custom designed. The cable is led off of the spool through the level winder, over and around the rear pulley, forward through the cable cutter, over the two remaining pulleys, and through an opening in the cradle to the anemometer (fig. 7). All pulleys are guarded with pins that prevent the cable from accidently coming out of the grooves of the pulleys, should slack develop. The pins and other details have been eliminated to reduce the clutter of nonessential details in figure 7. The rear pulley drives the eccentric cam by gears as shown in figure 7(a). The cam activates a microswitch which in turn activates the footage counters. The cable cutter is electrically actuated by a 1.0-A 1-W pyrotechnic (fig. 8), which is unfused and powered independently of the rest of the mechanism. The 2.0-A fuse in parallel with the cutter prevents its accidental firing from extraneous sources such as static electricity or radio-frequency fields. The cradle (fig. 5) is shaped and padded to receive the anemometer. The impact of cradling is appreciable; a distinct thud is noticed by passengers in a light-airplane installation. Although the cradling switch disconnects electrical power, both the anemometer and the spool of cable have considerable energy to be absorbed before coming to rest. Sponge rubber, about 12 mm thick was found to be satisfactory for stopping the anemometer.

The control of the mechanism is maintained with the operator's control box shown in figures 5 and 8. The control unit contains switches, indicator lamps, and cable footage counters. The power switch controls the 28 V to operate the mechanism. The deployment of the anemometer is controlled by the up-down switch in conjunction with the preset footage counter. The amount of cable to be deployed is entered in the preset counter, and the switch is moved to the down position. Additional cable can be let out in amounts indicated in the counter. Retraction continues until completion, or it may be interrupted by moving the switch to the off position. Power is removed when the anemometer reaches the cradle even if the up-down switch is left in the up position. The deployed footage counter indicates the total length of cable deployed; the power light, deployed light, maximum cable light, and cradled light indicate the circuit conditions. The cable cutter is controlled by the guarded switch on the control box and by a similar one on the box for the pilot. The operation of either switch activates the pyrotechnic-operated cutter which jettisons the anemometer if necessary.

Installation

The anemometer system can be attached directly to some airplanes, while with others, unavoidable wakes or ground-clearance problems require a bracket. (See fig. 9.) The combined mass of the anemometer and deployment mechanism is 7.80 kg.

The electrical connections are made with cables routed through the mounting flange, into the fuselage, to the control box, to the pilot's switch, to the recording system, and to the power source. In order to be consistent with the airplane instrumentation systems used at the Langley Research Center, the anemometer system was designed to operate from a 28-V direct-current source. A converter provides this power when instrumentation is installed in airplanes equipped with 12-V direct-current electrical systems.

RESULTS AND THEORETICAL DISCUSSION

Anemometer Accuracy

The principal anemometer calibration was made in an instrumentation-calibration wind tunnel that provides an airspeed range of approximately 0 to 90 m/sec. The closed test section is 0.762 m long and has a cross section 0.305 m by 0.432 m. Pitot-static measurements were made at 12 points in a cross-sectional plane ahead of the anemometer and at 12 corresponding points aft of the anemometer. The measurements were repeated with the anemometer removed from the test section. This procedure provides an accurate interpolation to the true airspeed at the propeller. Pressures from this pitot-static tube were measured with a precision barometer and a capacitive-type pressure gage to accuracies of $\pm$0.05 percent of full-scale range and $\pm$0.25 percent of reading, respectively. The temperature and humidity of the air were measured to accuracies of $\pm$0.5 K and $\pm$3 percent, respectively. True airspeed was determined by solving the equation

$$V = \sqrt{\frac{2q}{\rho}} \tag{1}$$

The value of air density ρ needed to solve equation (1) was determined by the equation

$$\rho = 1.225 \frac{t_o}{t} \frac{p - 0.3783e}{p_o} \tag{2}$$

With the measurement accuracies stated, true airspeed can be determined to within $\pm$0.15 m/sec over the full airspeed range. The accuracy of the calibration also depends on determining the airspeed at the propeller since the airspeed varies over the cross section and along the length of the test section. The frequency of the electrical output was measured with a precision frequency counter to an accuracy of $\pm$1.0 Hz, or approximately $\pm$0.08 percent of the full-scale range. The calibration data are plotted in figure 10 and show an average deviation of approximately $\pm$0.05 m/sec from the best straight line. The extended line does not pass through the origin but intersects the airspeed axis at about 0.25 m/sec. This offset is due to friction and magnetic loading of the tachometer (ref. 6). The results are repeatable so long as the anemometer is not damaged.

Misalinement of the longitudinal axis of the anemometer with the airstream results in a drop in output. The relationship between misalinement angle and error of output is shown in figure 11 for two airspeeds. The data show a 1.5-percent drop extending to approximately $\pm 10^{\circ}$, which is a characteristic of the propeller location and the shape and location of the shroud. The shroud design was selected from a number of designs tested. Correct static alinement was verified in wind-tunnel tests when the anemometer was suspended on the cable. Dynamic misalinement error was equivalent to statically measured error; dynamic response about the suspension axis was determined by measuring the free response to a pluck. The anemometer was mounted on an instrumented axle that provided a time history of angular position. Data from eight-airspeed conditions show that the natural frequency is proportional to the square root of the dynamic pressure;

that is,

$$f = 0.417\sqrt{q} \tag{3}$$

The damping is 7.3 percent of critical damping. Flight data containing oscillations of the frequency of equation (3) will be correctly read if the peak values are used. However, most flight data taken in clear air will not contain these fluctuations.

Errors arising from air-density variations due to altitude changes are characterized in propellers by shifts in the calibration curve, that is, with no change in the slope. (See ref. 7.) The intercept changes inversely as the square root of the density ratio. The intercept in the calibration, 4.5 Hz, is very small (fig. 10), this value being equivalent to 0.25 m/sec. Since the square root of the density ratio occurring between sea level and 3000 m varies from 1.0 to approximately 1.3, the intercept, or error, will remain small.

The low-temperature performance of the anemometer was verified by operating it in the exhaust stream of a compressed-air source. The temperature of the anemometer was lowered to 263 K and it continued to function normally for an extended period at that temperature. There is no temperature-sensitive component in the anemometer design that can affect its calibration or operation in a normal airplane environment.

Sufficient responsiveness of the propeller to dynamic inputs, such as gusts, was required to allow correlation with other recorded data. Measurement of the time constant was made from data taken in an open-jet wind tunnel at a number of representative airspeeds. The output of the propeller was recorded as it responded to the constant airstream after release from restraint. The data in figure 12 verify that the anemometer functions as a first-order system and that, at normal flying speeds, the anemometer lag is less than 0.1 sec. Phase or lag corrections can be made in correlating with other measurements, if required.

An overall value for the anemometer accuracy, including the sources of error discussed previously, is difficult to assign. The static calibration shows the anemometer is accurate to within ± 0.10 percent of full-scale output. Other sources of error, especially the effect of misalinement under small oscillations that may occur in flight, would suggest an accuracy of ± 0.50 percent of full scale may be more realistic in the flight environment. This value does not include errors arising from signal-conditioning and recording equipment used in flight, or from data reduction.

Cable Shape

The anemometer must be deployed into air that is undisturbed by the airplane. A separation of 1.5 wing spans measured between the airplane and the anemometer assures that the measured air is undisturbed. (See ref. 8.) The shape of the supporting cable always includes some sweepback due to wind resistance. A long cable supporting no weight on its end takes the form of a straight line, which is unstable. The trail-back angle increases with increasing airspeed (dynamic pressure). If a thin, flexible cable supports a fin-stabilized streamlined body, such

as in the present case, the shape is hyperbolic (shown in the photograph of fig. 13). The section of cable emerging from the anemometer is nearly normal to the airstream. Curvature is greatest on this end and decreases asymptotically to zero toward the attachment point. The determination of how much cable must be deployed to reach the undisturbed air can be done in a few steps.

Glauert, reference 9, has shown that the forces normal to an element of the flexible cable can be written

$$T \frac{d\phi}{ds} = -D \sin^2 \phi \tag{4}$$

where the bending of the cable is a function of drag. Equation (4) provides the needed relationships between the cable length s and the vertical separation z and the horizontal separation x from the attachment point and can be rewritten as

$$\frac{D}{T} s = \cot \phi = \sinh \frac{D}{T} z \tag{5}$$

and

$$\frac{D}{T} x = \cosh \frac{D}{T} z - 1.0 \tag{6}$$

The ratio D/T for the anemometer and cable in the present design is equal to $0.000057q$. Equation (5) can be used to determine the length of cable s needed to realize the required separation of 1.5 wing spans.

Calculations were made of cable shapes at several dynamic pressures and cable lengths. The shapes were compared with measurements obtained from photographs taken from a chase airplane. A sample comparison of the calculated and measured shapes is given in figure 14. The calculated shape has been corrected by an estimate of the effect of aerodynamic drag of the anemometer. The drag results in the cable emerging from the anemometer at an angle less than 90° from the horizontal. This initial angle is found by the relation (from ref. 9)

$$\phi_i = \tan^{-1} \frac{w}{D_a} \tag{7}$$

The anemometer drag D_a in equation (7) is the product of the impact pressure and a measured drag coefficient of 0.090. The value of the initial angle is used in equations (5) and (6) to compute the initial horizontal and vertical components x_i and z_i. These components locate the anemometer on the predicted shape, as indicated in figure 14.

Anemometer-Cable Dynamics

Loads suspended on cables beneath airplanes are subject to dangerous, divergent oscillations. These oscillations can be of two types: lateral-pendulum instability and cable whipping. Although the anemometer is a relatively small mass, there is a potential hazard to the deploying airplane and, should the cable break, to people and property on the ground. In addition, the oscillations in either mode generate velocity fluctuations which degrade the precision and accuracy of the airspeed measurement.

The boundaries of lateral-pendulum instability relating flight and anemometer parameters are given by reference 5 in the following two relationships:

$$\frac{Sqz}{wl} > \frac{1}{a\left[1 + \left(\frac{l}{k}\right)^2\right]} \tag{8}$$

and

$$\frac{Sqz}{wl} < \frac{C_D - a}{-aC_D}\left(\frac{k}{l}\right)^2 \tag{9}$$

Inequality (8) defines a lower limit of the lateral instability region which, in the case of the anemometer deployed at flight airspeeds, is a length so short (a few centimeters) as to be inconsequential. Essentially, the region of lateral instability extends from the initial deployment to the length defined by inequality (9). This instability is a phenomenon associated with deployment and retraction through the range of length; but since the cable lengthens during deployment, any lateral motion is lost as the critical length is exceeded. The amplitude of lateral oscillation which develop during retraction, however, tends to remain constant as the cable shortens, and may result in the anemometer missing the cradle and impacting the fuselage. If the airstream is uniform, this will not occur because natural oscillations build up slowly and retraction is accomplished while the amplitude is still inconsequential. If, however, the airstream contains either natural turbulence or turbulent wakes from airplane protuberances, the pendulum mode may be quickly excited to large amplitude.

Data from wind-tunnel tests defining the stability boundaries are plotted in figure 15, along with the predictions of inequalities (8) and (9). Data were taken at a number of airspeeds by noting the vertical lengths at which the induced lateral oscillations change from divergent to convergent, and vice versa. The transitions at very low airspeeds were sharply defined but became less so at higher airspeeds. At the lowest airspeed, the oscillations in the unstable lengths increased in amplitude at a rapid rate and were not confined to the lateral direction, but the motion became nearly circular in the horizontal plane. The upper stability boundary was poorly defined with a band of metastable lengths separating the clearly unstable from the clearly stable lengths. Data in figure 15 show that lateral-pendulum stability exists for cables longer than 4 m when towed at airspeeds of 20 m/sec or greater.

The lateral-pendulum stability of the anemometer was optimized with the fixed parameters of inequality (9) such as large tail surface, tail length, tail lift slope, and small mass and radius of gyration. The rugged, lightweight tail has a large area with favorable lift characteristics. The tail length is short to minimize the radius of gyration which influences stability in proportion to the second power. The mass is not minimized to gain stability but is made as large as possible to achieve maximum separation between the airplane and the anemometer for a given cable length.

Cable whipping is another mode of oscillatory motion that has produced problems for suspended bodies. In reference 10, it was found that this condition arose when disturbances picked up near the airplane attachment point acquired additional energy as they traveled down the cable when the airspeed exceeded the speed of propagation of waves along the cable. As the airspeed increased beyond this critical speed, the amplification increased and caused the cable to fail. The disturbance may arise from wakes from protrusions upstream of the airplane attachment point, from prop wash, and from natural turbulence. The problem can be minimized if care is taken in selecting the attachment point for the deployment mechanism. Calculations made by using the methods of reference 10 and the parameters of the anemometer predict cable-whipping instability at airspeeds above 65 m/sec (130 knots), although it has not been demonstrated in flight.

CONCLUDING REMARKS

A suspended anemometer system is described which is used to calibrate pitot-static systems on low-speed airplanes. The anemometer senses true free-stream airspeed when suspended in regions of undisturbed air. The anemometer is particularly well suited for the application because of the following characteristics:

1. The output is a self-generating, alternating voltage whose frequency is a linear function of true airspeed over the desired range of 20 to 60 m/sec (40 to 120 knots).

2. The accuracy of the measurement is within $\pm$0.50 percent of the full-scale range. This value excludes errors arising from signal-conditioning and recording instrumentation.

3. The anemometer output is unaffected by air density or by the temperature for the normal airplane environment.

4. Conditions of lateral-pendulum instability of the anemometer-cable system were investigated, and stable conditions were shown to exist over the airspeed range with cable lengths over 4 m. Cable-whipping instability is predicted, although not demonstrated at airspeeds above 65 m/sec (130 knots).

Langley Research Center
National Aeronautics and Space Administration
Hampton, VA 23665
August 17, 1977

REFERENCES

1. Jordan, Frank L., Jr.; and Ritchie, Virgil S.: Subsonic Wind-Tunnel Tests of a Trailing-Cone Device for Calibrating Aircraft Static-Pressure Systems. NASA TN D-7217, 1973.

2. Coleman, Donald G.: N.A.C.A. Flight-Path-Angle and Air-Speed Recorder. NACA TN 233, 1926.

3. Beij, K. Hilding: Aircraft Speed Instruments. NACA Rep. 420, 1932.

4. Fisher, Bruce, D.; Stough, H. Paul; and Kershner, David D.: Trailing Anemometer for Low Airspeed Calibration. [Preprint] 760 461, Soc. Automot. Eng., Apr. 1976.

5. Phillips, W. H.: Stability of a Body Stabilized by Fins and Suspended From an Airplane. NACA ARR L4D18, WRL-28, 1944.

6. Zahm, A. F.; Smith, R. H.; and Louden, F. A.: Drag of C-Class Airship Hulls of Various Fineness Ratios. NACA Rep. 291, 1928.

7. Ower, E.: The Measurement of Air Flow. Third ed. Chapman & Hall, Ltd. (London), 1949.

8. Thompson, F. L.: The Measurement of Air Speed of Airplanes. NACA TN 616, 1937.

9. Glauert, H.: Heavy Flexible Cable for Towing a Heavy Body Below an Aeroplane. R. & M. No. 1592, British A.R.C., 1934.

10. Phillips, Williams H.: Theoretical Analysis of Oscillations of a Towed Cable. NACA TN 1796, 1949.

L-73-2216

Figure 1.- Suspended anemometer.

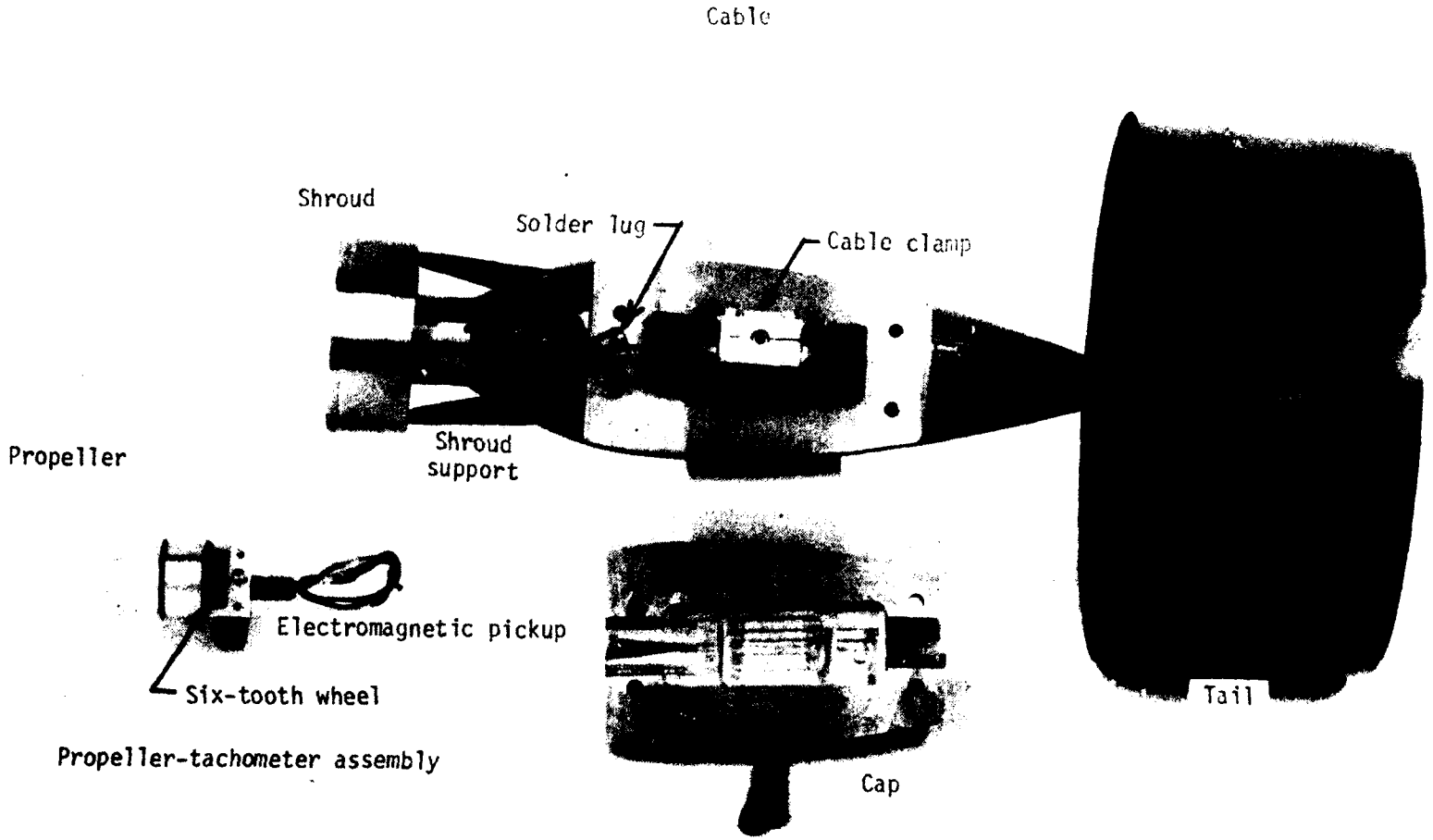

L-73-1663.1

Figure 2.- Partially disassembled anemometer.

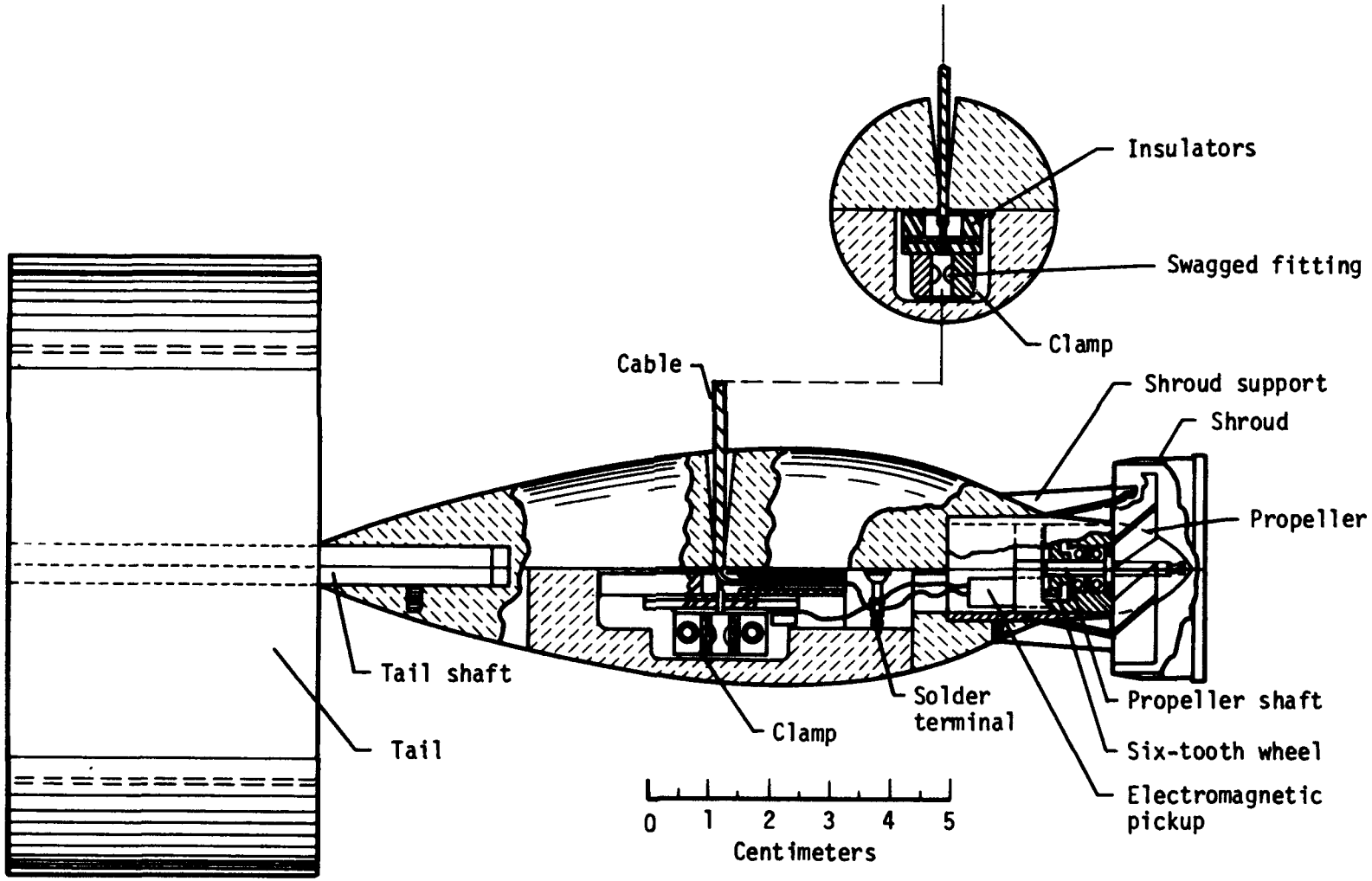

Figure 3.- Ai. ometer body.

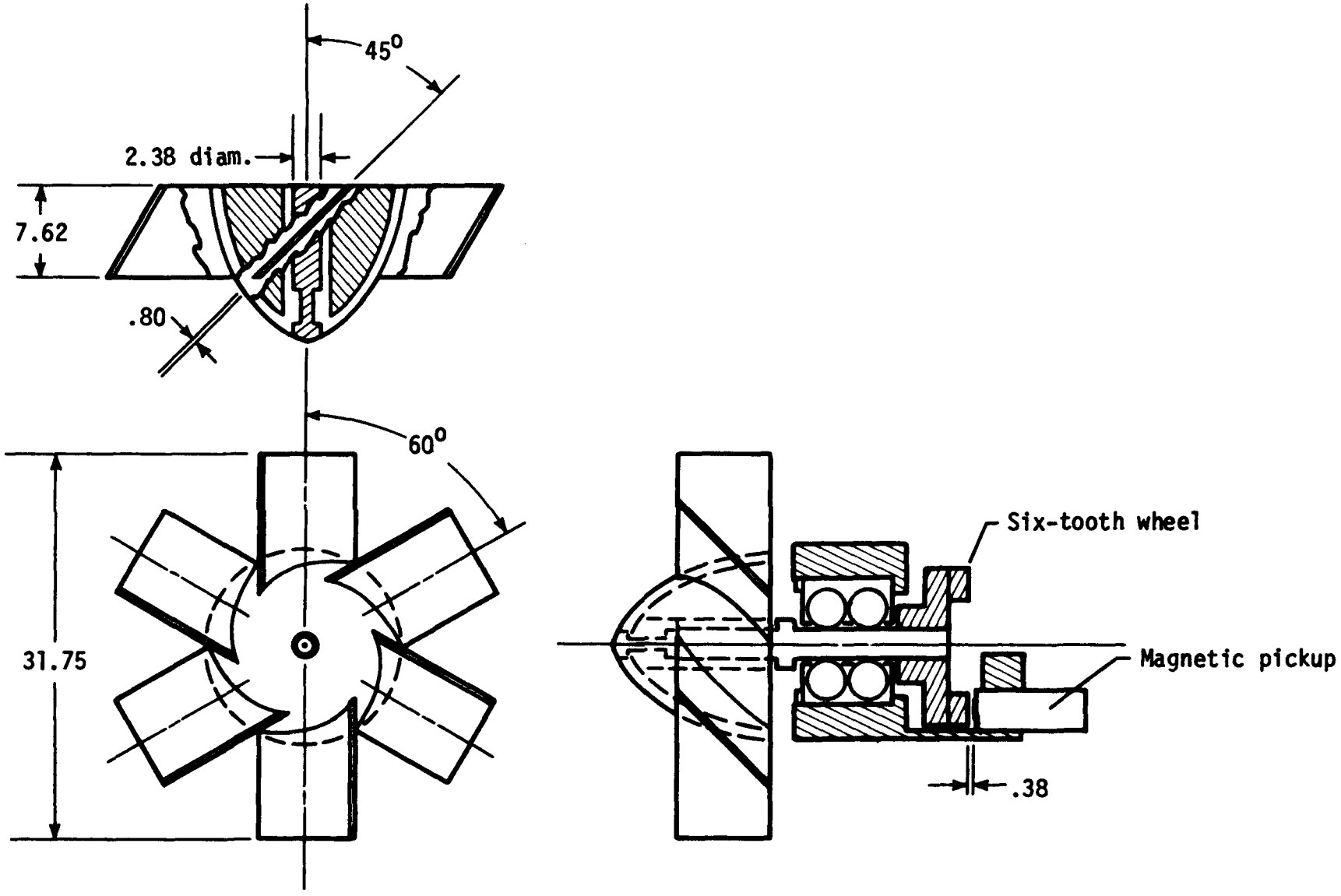

Figure 4.- Propeller-tachometer assembly. (Linear dimensions are in mm.)

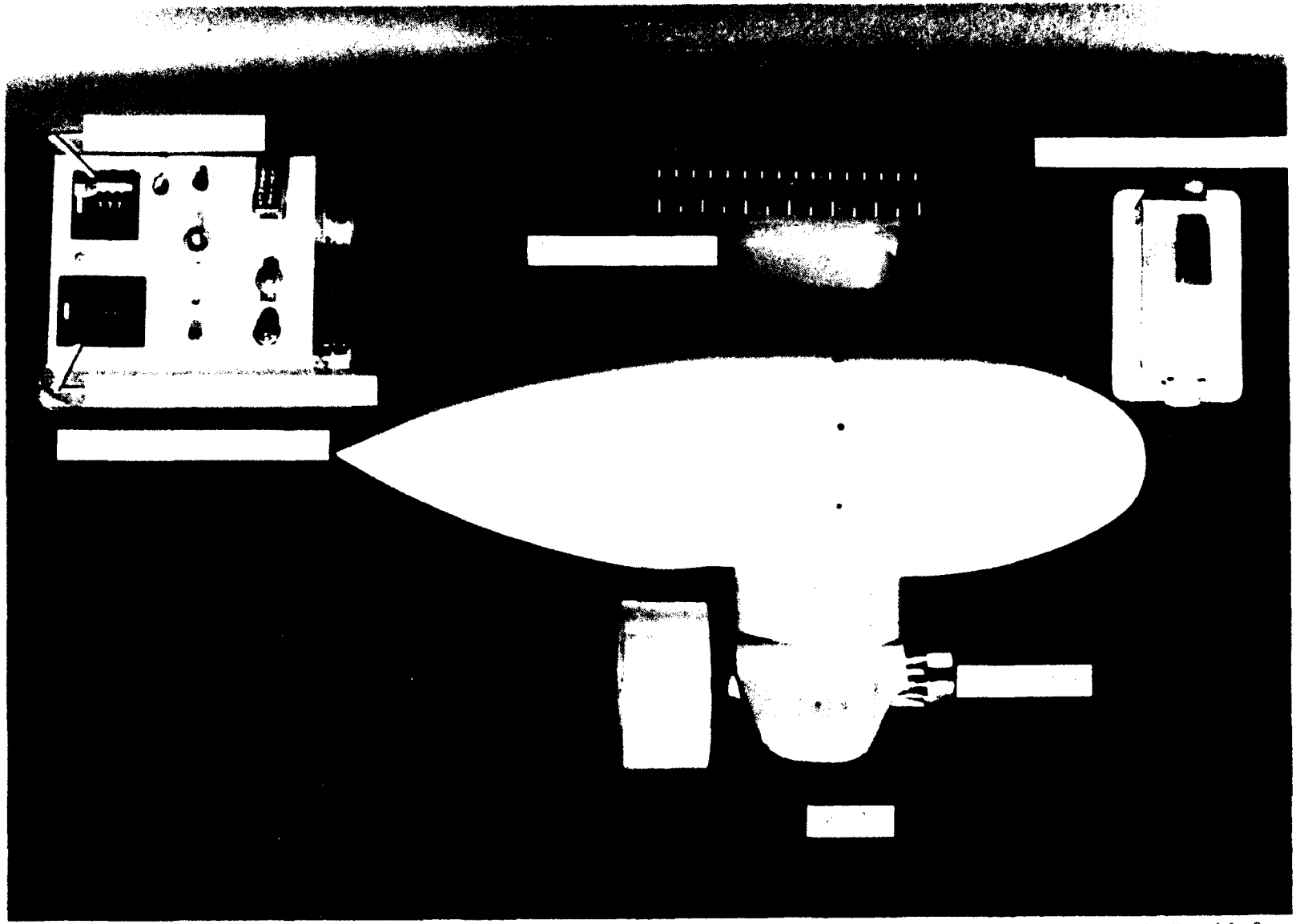

L-73-6658.1

Figure 5.- Complete system with anemometer retracted.

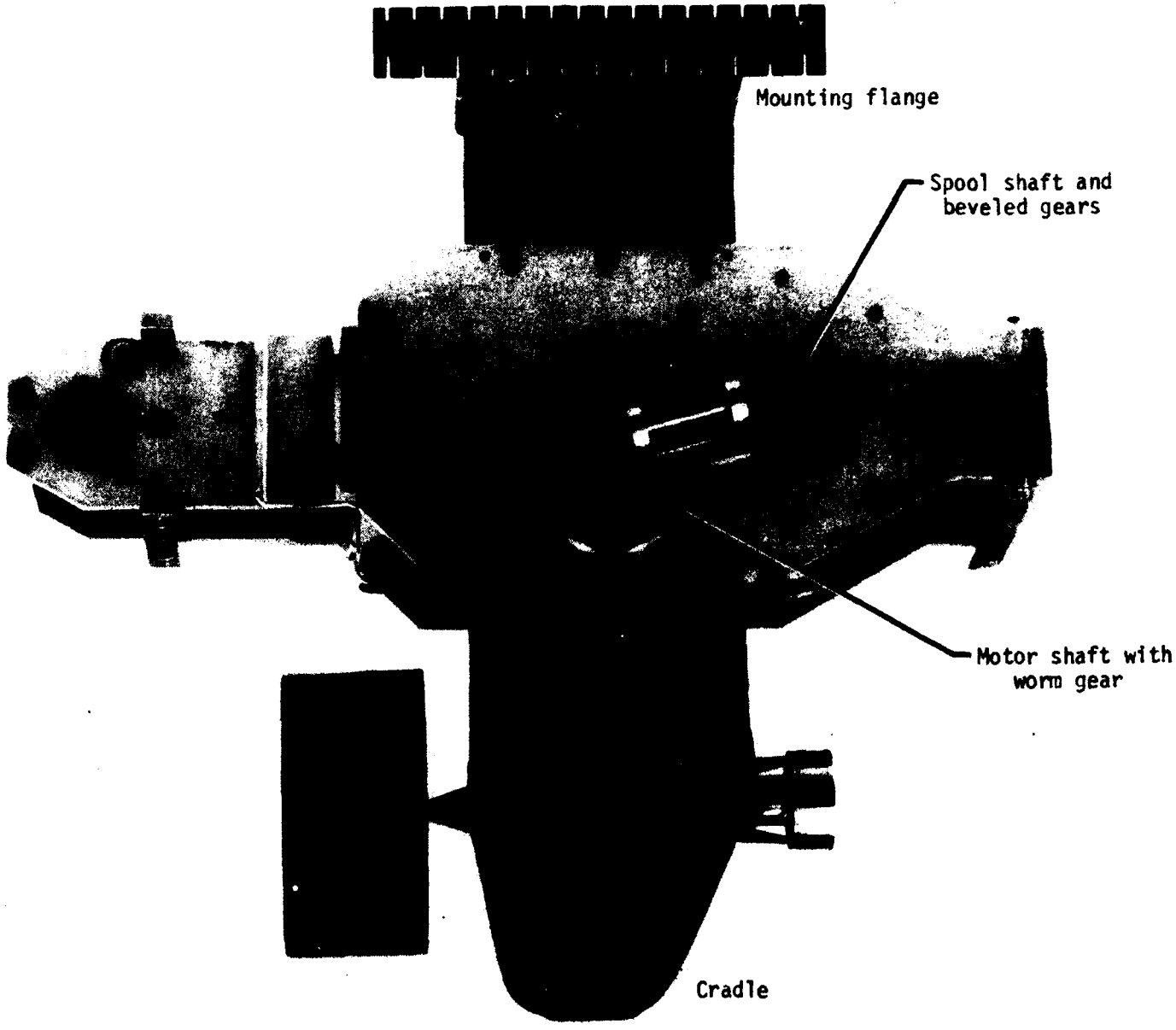

(a) Right side.

Figure 6.- Deployment mechanism with cover removed.

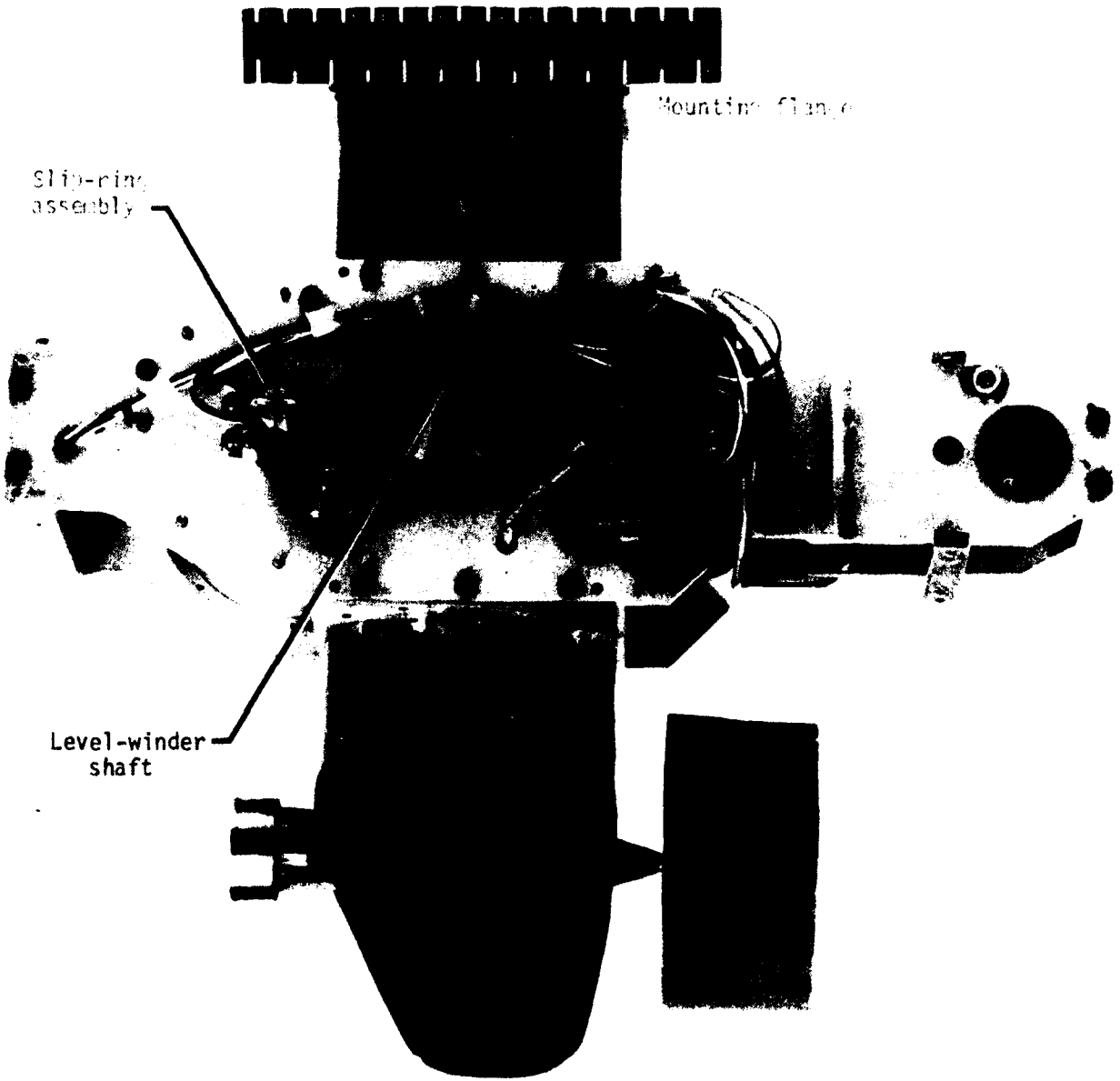

L-73-5784.1

(b) Left side.

Figure 6.- Concluded.

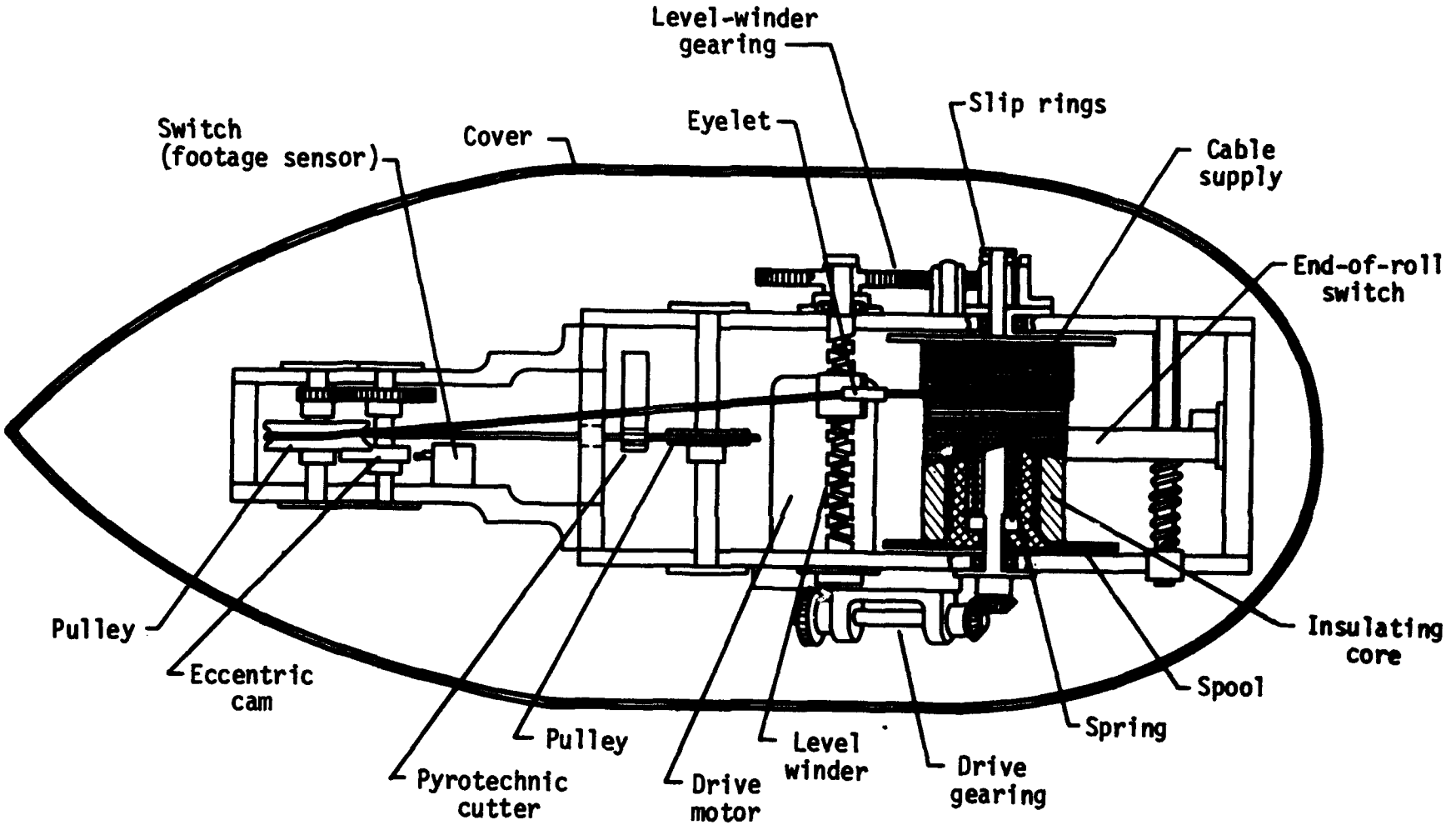

(a) Top view.

Figure 7.- Deployment mechanism.

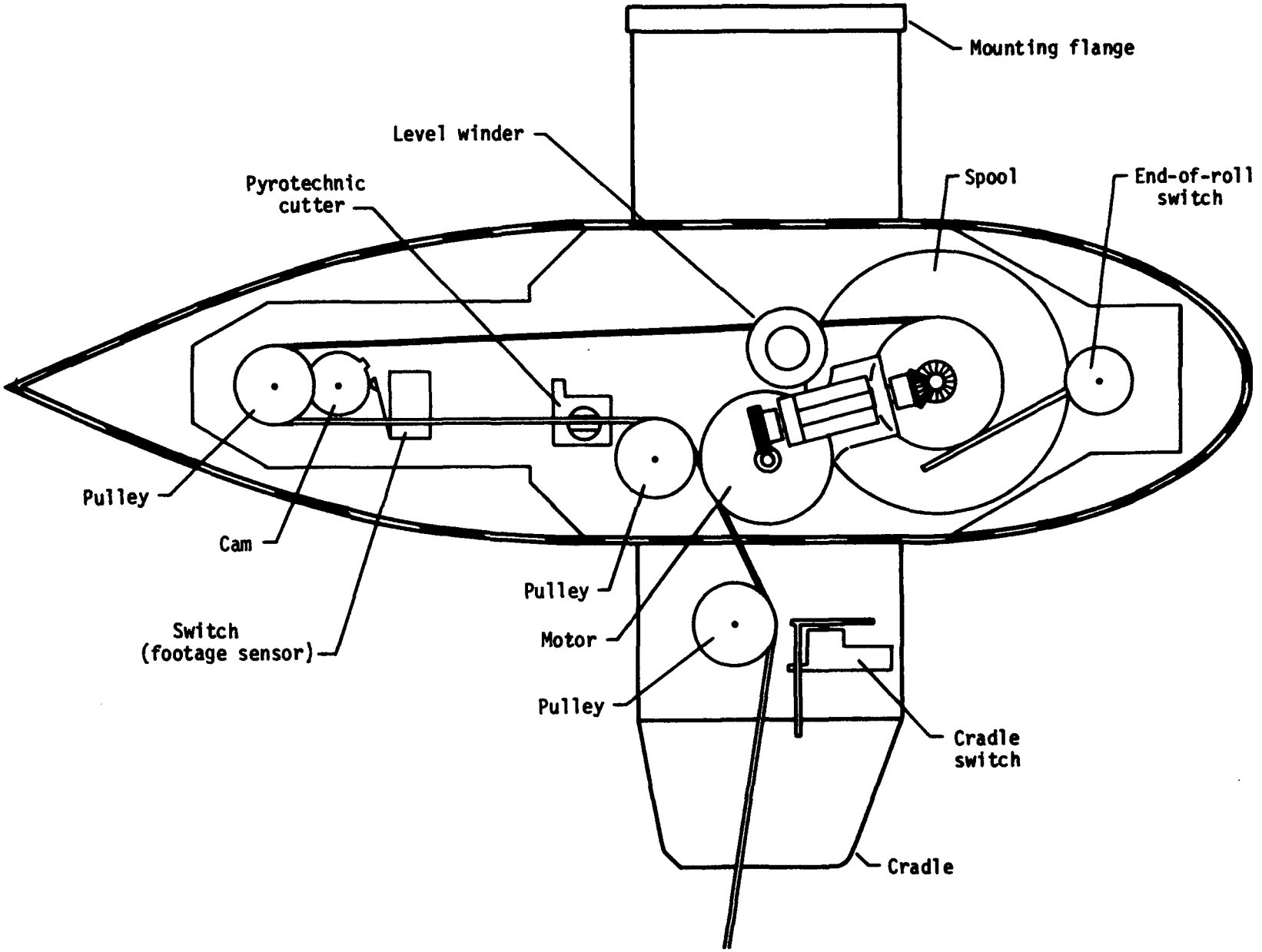

(b) Side view.

Figure 7.- Concluded.

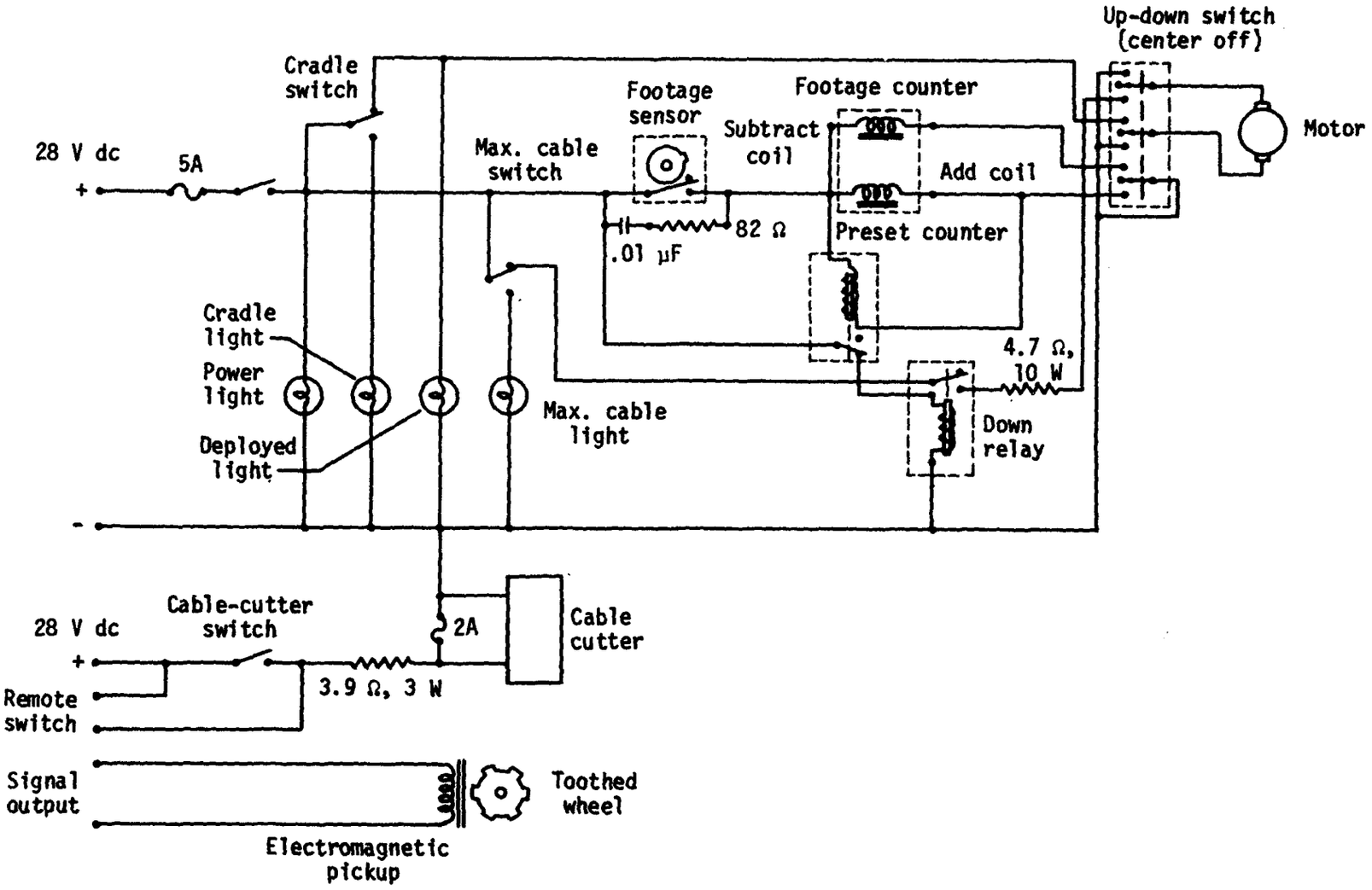

Figure 8.- Schematic of electrical system.

L-76-3518

(a) Mounted directly to bottom of fuselage.

L-76-2209

(b) Side mounted with brackets.

Figure 9.- Installation of deployment mechanism.

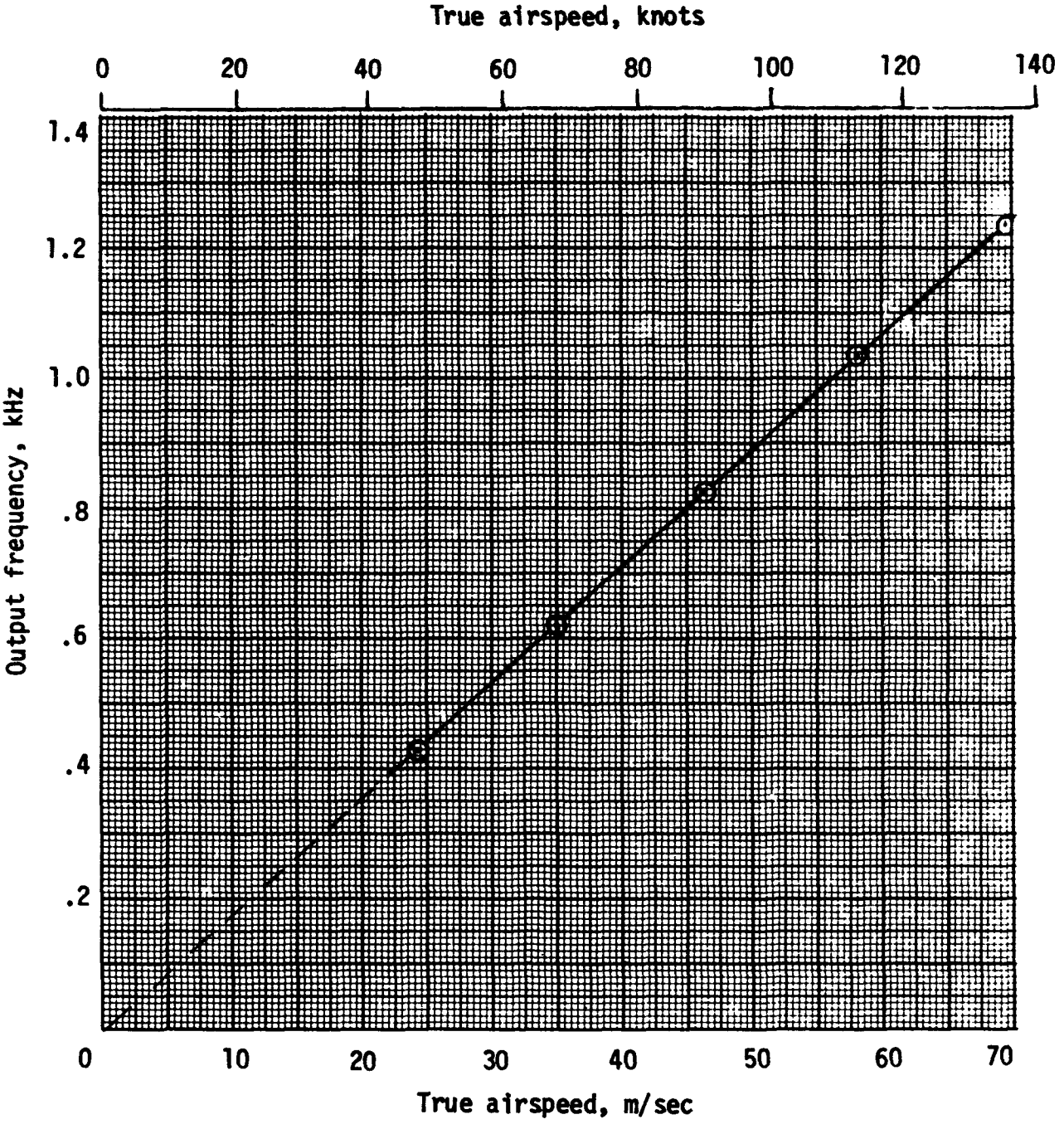

Figure 10.- Anemometer calibration based on wind-tunnel cross-section velocity profile.

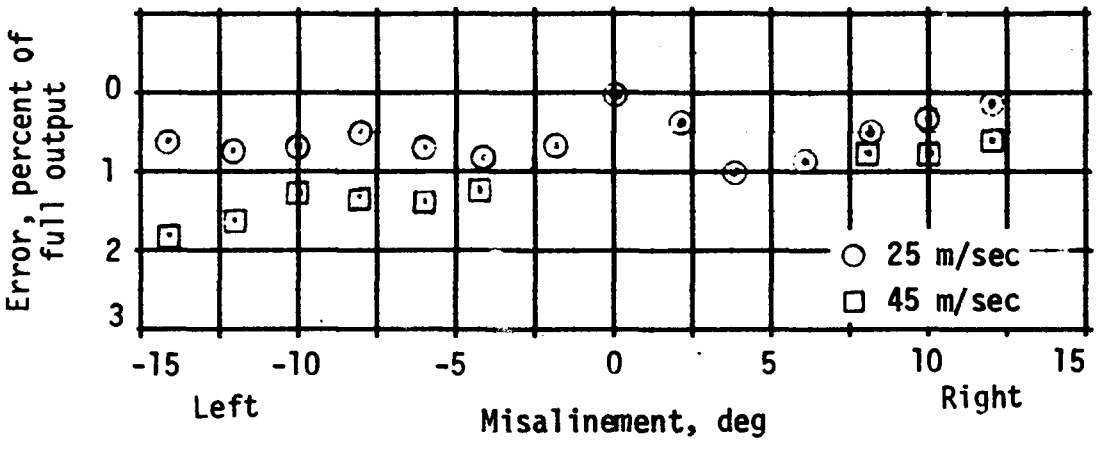

Figure 11.- Variation of anemometer output with misalinement.

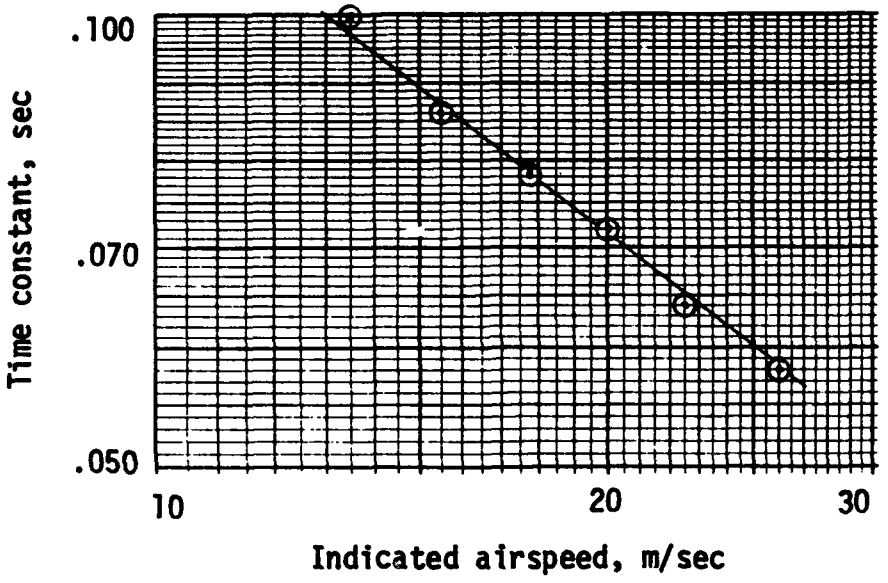

Figure 12.- Variation of anemometer time constant with indicated airspeed.

L-74-1817

Figure 13.- Anemometer suspended from light airplane. (Image of cable has been enhanced.)

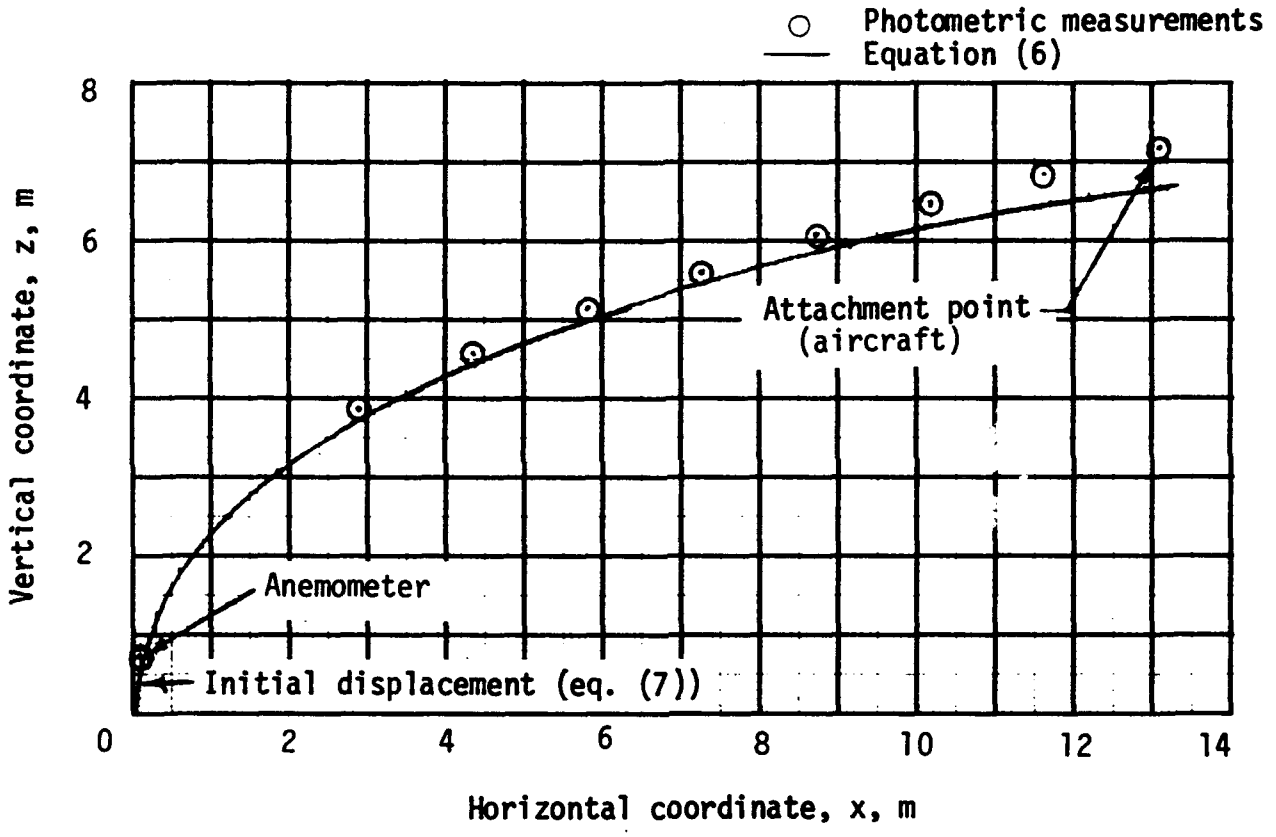

Figure 14.- Shape of anemometer cable when operating at dynamic pressure of 1.93 kPa with 17 m of cable deployed.

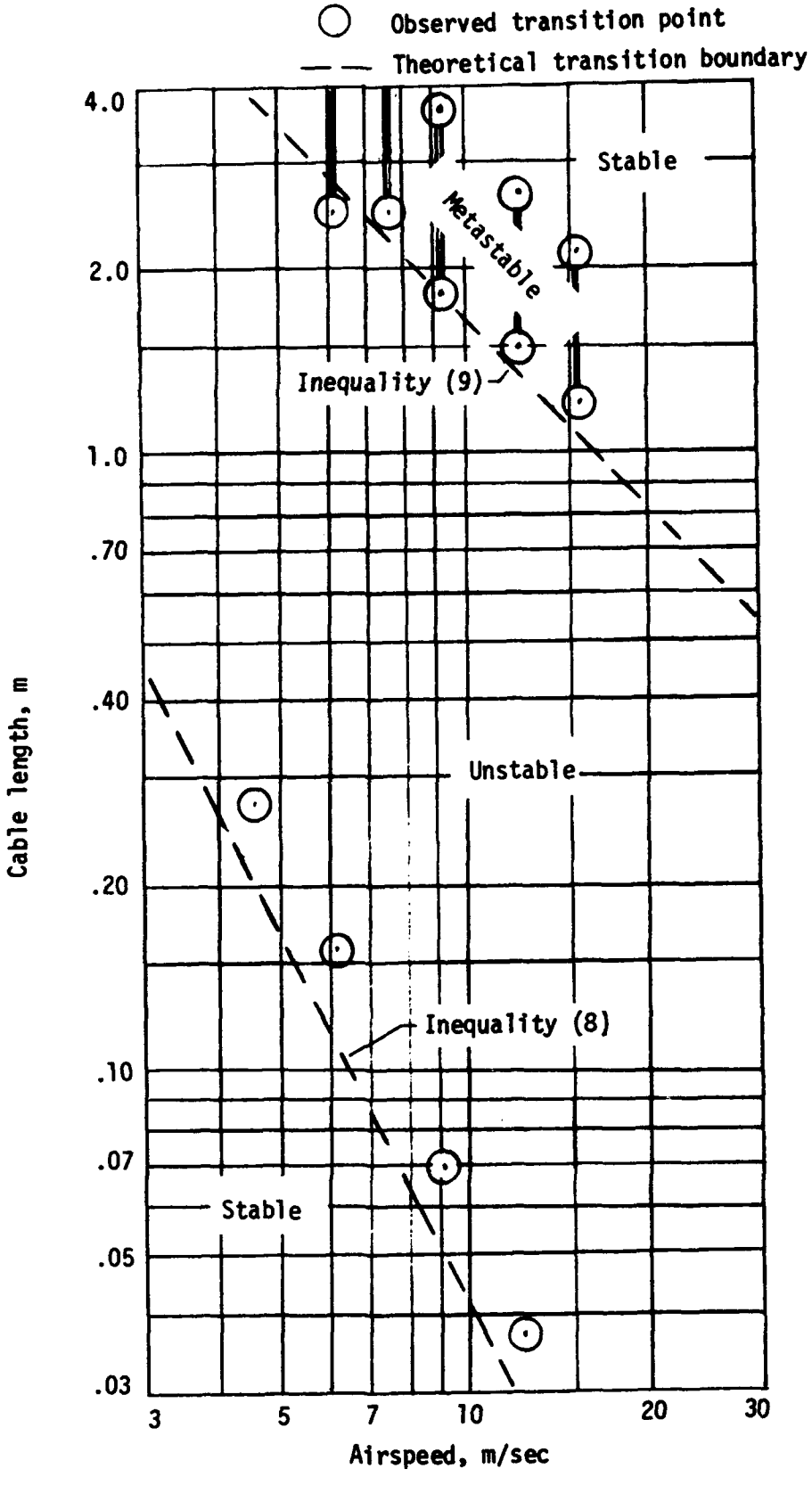

Figure 15.- Comparison of theoretical and observed lateral-pendulum stability of anemometer.

NASA-Langley, 1977 L-11269